

# A novel perspective to high-speed cross-hot-wire calibration methodology

B. Cukurel · S. Acarer · T. Arts

Received: 23 September 2011 / Revised: 18 June 2012 / Accepted: 22 June 2012 / Published online: 14 July 2012  
© Springer-Verlag 2012

**Abstract** A practical cross-hot-wire calibration and data reduction methodology for instantaneous measurements of mass flux and flow angle is developed for two dimensional subsonic compressible flows. Historically, data reduction for flow conditions of  $0.4 < M < 1.2$  is regarded as problematic, even in the simplified case of flow normal mounted wires. Thus, in comparison with the incompressible and supersonic conditions, the literature addressing these flow regimes is quite limited. The present study addresses this void by relating the wire voltages to flow conditions through renormalized, Mach and overheating independent, nondimensional quantities. Therefore, a short and robust calibration can be performed in an unheated free jet facility with applicability toward a broad range of planar flow conditions. This disposes the need for typical closed loop calibration wind tunnels which vary flow velocity, density and temperature independently to parameterize the voltage dependency in a purely empirical manner.

## List of symbols

|            |  |
|------------|--|
| $A$        | Area   |
| $a_0, a_1$ | Resistance temperature coefficients (Eq. 17) |
| $d_w$      | Wire diameter                                |
| $E_b$      | Bridge voltage                               |
| $E_w$      | Wire voltage                                 |
| $Gr$       | Grashof number                               |
| $k$        | Thermal conductivity                         |

|            |   |
|------------|---|
| $Kn$       | Knudsen number $M/Re\sqrt{0.5\rho g\pi}$  |
| $l_a$      | Active wire length  |
| $l_t$      | Total wire length   |
| $m$        | $(1 + (\gamma - 1)/2M^2)^{-1}$  |
| $M$        | Mach number   |
| $Nu$       | Nusselt number  |
| $P$        | Pressure  |
| $Pr$       | Prandtl number  |
| $q$        | Convective heat transfer rate   |
| $Re$       | Reynolds number   |
| $R_g$      | Gas constant  |
| $R_l$      | Lead's resistance   |
| $R_t$      | Bridge top resistance   |
| $R_{Tu}$   | Correlation coefficient between fluctuations in static temperature and velocity |
| $R_w$      | Wire resistance   |
| $S_\alpha$ | Angular sensitivity   |
| $S_{To}$   | Total temperature sensitivity   |
| $S_u$      | Velocity sensitivity  |
| $S_\rho$   | Density sensitivity   |
| $T$        | Temperature   |
| $T_r$      | Adiabatic wire temperature  |
| $T_w$      | Wire temperature  |
| $u$        | Velocity (magnitude)  |

## Greek

|             |  |
|-------------|--|
| $\varphi$   | Correction factor (Eq. 18)               |
| $\gamma$    | Gas specific heat ratio                  |
| $\theta$    | Overheat ratio, $T_w/T_0$                |
| $\beta$     | Pitch angle                              |
| $\alpha$    | Yaw angle                                |
| $\tau_{wr}$ | Overheating parameter, $(T_w - T_r)/T_r$ |
| $\eta$      | Recovery factor, $T_r/T_0$               |
| $\mu$       | Dynamic viscosity                        |
| $\rho$      | Density                                  |

B. Cukurel (✉) · S. Acarer · T. Arts  
von Karman Institute for Fluid Dynamics,  
Chaussée de Waterloo, 72, 1640 Rhode-St-Genèse, Belgium  
e-mail: cukurel@vki.ac.be

## Abbreviations

|           |  |
|-----------|--|
| CCA       | Constant current anemometry                                  |
| CTA       | Constant temperature anemometry                              |
| CVA       | Constant voltage anemometry                                  |
| HWA       | Hot-wire anemometry  |
| rms, nrms | Non-normalized and local mean-normalized “root mean squared” |

## Subscripts

|      |                   |
|------|-------------------|
| 0    | Total conditions  |
| 1, 2 | Wire numbers      |
| corr | Corrected         |
| eff  | Effective         |
| ins  | Instantaneous     |
| ref  | Reference         |
| s    | Static conditions |

## Special symbols

|       |  |
|-------|--|
| $()'$ | Fluctuating quantity, for example $u' = u - \bar{u}$ |
| $()$  | Time averaged quantity                               |

## 1 Introduction

Historically, one of the principal means to measure instantaneous turbulent flow quantities at high frequency is hot-wire anemometry (HWA), a technique which relates heated thin wire convection to the consumed electrical power. There are three types of control circuits feeding electrical current to the wire, the two common modes being constant current (CCA) and constant temperature (CTA) (Brunn 1995), whereas the third developing type is the constant voltage (CVA) (Kegerise and Spina 2000). For the entire subsonic and transonic flow range, due to its well-established technology, reliability and ease of use, CTA is the standard control unit, a wheatstone circuit where the exposed sensory element constitutes a leg of the bridge. The wire temperature, and equivalently resistance, is fixed at a value higher than the surrounding fluid (overheating) by a fast response feedback amplifier, which corrects the bridge voltage unbalance by modifying the circuit top voltage. Therefore, by maintaining a constant wire resistance with respect to the other internal arms of the bridge, CTA eliminates thermal inertia issues (Brunn 1995), and thus, the wire heat transfer can be directly related to the bridge top voltage.

### 1.1 Heat transfer over heated thin wires

In general, heat transfer from heated thin wires in high-speed flows is a complex phenomenon depending on various parameters such as wire temperature and geometry, flow velocity, density and temperature. In low-speed

applications, compressibility effects can be ignored and well-known simplified relationships, such as King’s Law, can be used to relate flow velocity to the bridge voltage, possibly in conjunction with temperature correction methods (Brunn 1995). However, in the presence of compressibility effects, in addition to velocity, density and total temperature may also fluctuate significantly, coupling the relations. Furthermore, in subsonic and transonic flows, the heat transfer is strongly dependent on Mach number, despite being negligible for  $M > 1.4$  (Stainback and Nagabushana 1993). Such difficulties resulted in lack of reliable measurements within this regime until the late 1970 s.

In high subsonic and transonic flows, one approach to quantify the voltage dependency of the hot-wire signal is to assume a functional dependency of  $E_b = f(\rho, u, T_0)$  for a given probe and wire temperature, and empirical curve-fitting these variables by multiregression methods. A technique more physical in nature is to determine the sensitivity to various nondimensional parameters, which also comprises the bases of the presented investigation.

In the most general sense, the convective heat transfer from the wire to the gas can be expressed in terms of Nusselt number (Morkovin 1956), typically defined as,

$$Nu = \frac{q}{\pi l_a k (T_w - \eta T_0)} \quad (1)$$

where  $l_a$  and  $\eta$  are active wire length and recovery factor, respectively. A Buckingham-Pi analysis of steady heat transfer from heated thin wires yields to Nusselt number dependency on free stream Reynolds, Prandtl, Mach, and Grashof numbers, in addition to yaw angle ( $\alpha$ ), pitch angle ( $\beta$ ), and wire length-to-diameter ratio. For a more complete functional relationship to incorporate the effects of the momentum/thermal boundary layers around the cylinder, the overheating dependency should also be included (Stainback and Nagabushana 1993), resulting in:

$$Nu = f(Re, Pr, M, Gr, \tau_{wr}, \alpha, \beta, l_a/d_w) \quad (2)$$

where Reynolds number is defined as,

$$Re = \frac{\rho u d_w}{\mu} \quad (3)$$

In addition, there is a strong Knudsen number influence on heat transfer due to small wire diameters in combination with high velocities and/or low densities, which may cause a deviation from the continuum flow ( $Kn > 0.01$ ). Due to this kind of gas rarefaction effects, considering  $Kn = (\rho g \pi / 2)^{0.5} M / Re$  (Brunn 1995), the Mach number dependency of the Nusselt number has been observed to extend far below the typical incompressibility limit of  $Ma \sim 0.3$ , even to values as low as 0.05 (Spangenberg 1955).

For a given probe geometry ( $l_x/d_w$ ), in a planar flow field ( $\beta$ ) of a specific gas ( $Pr$ ), with negligible natural convection (for  $Re > Gr^{0.3}$ ), and overheating dependency ( $\Delta\theta$  effect negligible for “moderate” changes of total temperature in CTA mode (Dewey 1965), as will be addressed in Sects. 2.4 and 2.5), Eq. 2 can be simplified to:

$$Nu = f(Re, M, \alpha). \tag{4}$$

Similarly, due to imperfect stagnation of flow over the wire, it has been observed (Brunn 1995) that the recovery factor of the wire ( $\eta$ ) is also a function of:

$$\eta = f(Re, M, \alpha). \tag{5}$$

There are few compressible flow studies that quantify the functional dependencies of  $Nu$  and  $\eta$  on their respective independent variables, while the relationships are empirically based (Dewey 1965; Behrens 1971).

### 1.2 Compressible flow turbulence measurements

Having considered the more generalized problem of flow over heated thin wires, the historic adaptation of this theory to hot-wire anemometry has been investigated in literature. Pioneering work on application of one-dimensional flow normal hot-wire methods for supersonic flows were conducted by Kovaszny (1950, 1953) and Morkovin (1956) for CCA operation. These methods are based on a sensitivity analysis assuming small perturbations, where the percent bridge voltage variation is decomposed to percent fluctuations in density, velocity and total temperature:

$$\frac{E'_b}{E_b} = S_\rho \frac{\rho'}{\rho} + S_u \frac{u'}{u} + S_{T_0} \frac{T'_0}{T_0} \tag{6}$$

where  $S_\rho$ ,  $S_u$ , and  $S_{T_0}$  are sensitivity to density, velocity and total temperature respectively; defined as:

$$S_\rho(\rho, u, T_0) = \left. \frac{\partial \log E_b}{\partial \log \rho} \right|_{u=\text{const.}, T_0=\text{const.}} \tag{7a}$$

$$S_u(\rho, u, T_0) = \left. \frac{\partial \log E_b}{\partial \log u} \right|_{\rho=\text{const.}, T_0=\text{const.}} \tag{7b}$$

$$S_{T_0}(\rho, u, T_0) = \left. \frac{\partial \log E_b}{\partial \log T_0} \right|_{\rho=\text{const.}, u=\text{const.}} \tag{7c}$$

Following Morkovin’s terminology, using Eqs. 4 and 5, the CTA sensitivity expressions for a flow normal wire can be derived by logarithmic differentiation of Eq. 1 (Nagabushana and Stainback 1992):

$$S_\rho = \frac{1}{2} \left( \frac{\partial \log Nu}{\partial \log Re} - \frac{1}{\tau_{wr}} \frac{\partial \log \eta}{\partial \log Re} \right) \tag{8a}$$

$$S_u = S_\rho + \frac{1}{2m} \left( \frac{\partial \log Nu}{\partial \log M} - \frac{1}{\tau_{wr}} \frac{\partial \log \eta}{\partial \log M} \right) \tag{8b}$$

$$S_{T_0} = \frac{1}{2} \left[ n_t + 1 - m_t \frac{\partial \log Nu}{\partial \log Re} - \frac{\theta}{\theta - \eta} + \frac{1}{\tau_{wr}} \left( -\frac{1}{2m} \frac{\partial \log \eta}{\partial \log M} + m_t \frac{\partial \log \eta}{\partial \log Re} \right) - \frac{1}{2m} \frac{\partial \log Nu}{\partial \log M} \right] \tag{8c}$$

where  $n_t = \partial \log k / \partial \log T_0$  and  $m_t = \partial \log \mu / \partial \log T_0$ . If necessary, similar sensitivity expressions could also be derived by using other equivalent functional relationships such as  $Nu = f(M, Kn)$  and  $\eta = f(M, Kn)$ , reviewed by Stainback and Nagabushana (1993).

These sensitivities can either be obtained directly in close loop wind tunnel facilities by methodically varying one independent parameter while holding the others constant at each mean value (Eqs. 7a, 7b, 7c or 8a, 8b, 8c), which is impractical (direct methods), or mathematically in the presence of closed form formulations (indirect methods) (Horstman and Rose 1975), such as the ones proposed by Dewey (1965) or Behrens (1971). However, these universal correlations are only valid for infinitely long ideal wires. Therefore, even in the presence of end-loss corrections, as proposed by Dewey (1961) and Lord (1974), despite preserving the trends, it is shown that the wire-specific calibrations provide more accurate results (Horstman and Rose 1975).

The instantaneous solution of Eq. 6 requires using a three wire probe, where each wire has sufficiently different sensitivities to create a nonsingular solution matrix with known sensitivities (Stainback and Johnson 1983; Jones et al. 1989). However, this kind of instantaneous solution of fluctuations was questioned by Walker et al. (1988), who concluded that although the instantaneous wire voltages correlate well, minute errors in signals cause large errors on the resulting mass-flux and total temperature fluctuations.

Nevertheless, the concentration of most prior literature was toward obtaining time averaged turbulent quantities rather than their instantaneous values. Therefore, Eq. 6 is typically modified to provide the mean-squared sensitivity equation for flow normal mounted wires:

$$Re \frac{\overline{E_b'^2}}{(\overline{E_b})^2} = S_\rho^2 \left[ \frac{\overline{\rho'^2}}{\overline{\rho}^2} \right] + S_u^2 \left[ \frac{\overline{u'^2}}{\overline{u}^2} \right] + S_{T_0}^2 \left[ \frac{\overline{T_0'^2}}{(\overline{T_0})^2} \right] + 2S_u S_{T_0} \left[ \frac{\overline{u' T_0'}}{\overline{u T_0}} \right] + 2S_\rho S_{T_0} \left[ \frac{\overline{\rho' T_0'}}{\overline{\rho T_0}} \right] + 2S_\rho S_u \left[ \frac{\overline{\rho' u'}}{\overline{\rho u}} \right]. \tag{9}$$

Kovaszny (1950) observed that sensitivities, although weak, are a function of wire temperature and thus overheat; hence, it is possible to solve Eq. 9 by varying the overheat

ratio, assuming that statistical flow properties remain constant. More specifically, by means of a single wire with at least six different overheat ratios, using Eq. 9 with predetermined sensitivities, the six unknowns can be computed,  $(\overline{\rho'^2}/\overline{\rho}^2)$ ,  $(\overline{u'^2}/\overline{u}^2)$ ,  $(\overline{T_0'^2}/\overline{T_0}^2)$ ,  $(\overline{u'T_0'}/\overline{uT_0})$ ,  $(\overline{\rho'T_0'}/\overline{\rho T_0})$  and  $(\overline{\rho'u'}/\overline{\rho u})$ . However, in practice, this is almost impossible because even very small errors in obtaining the sensitivities cause an ill conditioning of the matrix (Stainback and Nagabushana 1995).

Alternatively, it has been shown that if the wire normal Mach number component is greater than 1.2, then the heat transfer is independent of the Mach number (Morkovin 1956), therefore  $\partial/\partial M = 0$  in Eqs. 8a, 8b, 8c, resulting in an equality between the density and velocity sensitivities ( $S_u = S_\rho$ ). Therefore, Eq. 6 becomes:

$$\frac{E'_b}{E_b} = S_{\rho u} \frac{\rho u'}{\rho u} + S_{T_0} \frac{T_0'}{T_0} \quad (10)$$

which is only dependent upon mass-flux and total temperature fluctuations. Through mean squaring of the quantities, the equation can be reformatted to provide:

$$\frac{\overline{E_b'^2}}{(\overline{E_b})^2} = S_{\rho u}^2 \left[ \frac{(\overline{\rho u})'^2}{(\overline{\rho u})^2} \right] + S_{T_0}^2 \left[ \frac{\overline{T_0'^2}}{(\overline{T_0})^2} \right] + 2S_{\rho u}S_{T_0} \left[ \frac{(\overline{\rho u})'T_0'}{(\overline{\rho u})\overline{T_0}} \right]. \quad (11)$$

By these reduced three unknowns, Kovaszny (1953) developed the 'fluctuation diagram technique', a graphical method, to solve Eq. 11. Although three different overheat ratios are sufficient to solve this equation, accuracy can be improved by using more overheat levels by rapid scanning. In the face of prior unsuccessful attempts at extending these techniques to CTA operation, Smits et al. (1983) associate the cause of implementation inadequacy to the decrease in system linearity, stability and frequency response with the reducing overheat. Therefore, CTA is only suitable for high (and single) overheat ratio operations where  $S_{T_0}$  is low and  $S_u$  and  $S_\rho$  (or  $S_{\rho u}$ ) are high. Instead, in CTA operation, if total temperature fluctuations are small (e.g., in adiabatic flows) or if the wire is insensitive to such fluctuations [true for  $\theta > 2.5$  (Horstman and Rose 1975; Mikulla and Horstman 1975)], then the temperature terms in Eqs. 9 and 11 vanish, greatly simplifying the equations.

However, at compressible subsonic and transonic flow regimes, due to the strong Mach number dependency, the equality between the density and velocity sensitivities vanishes ( $S_u \neq S_\rho$ ); thus, the simplification from Eqs. 9 to 11 is inapplicable. In literature, there exists a large inconsistency regarding the significance of this inequality. For example, some experimental studies (Horstman and Rose 1975; Johnson and Rose 1976; Rose and McDaid 1977; Rong et al. 1985) indicated that the Mach number effect in

these regimes can be negligible if overheating  $\theta > 1.5$  and  $Re > 20$ . Therefore, the density sensitivity is very close to the velocity sensitivity. This is contrasted by Nagabushana and Stainback (1992), Stainback and Johnson (1983), Jones et al. (1989), who clearly state strong Mach number effects, therefore  $S_u \neq S_\rho$ . In summary, most investigators had to assume  $S_u = S_\rho$  to obtain the fluctuation information from their respective data sets (Motallebi 1994).

If mass flux can be calculated accurately in a flow environment absent of significant total temperature fluctuations (isentropic), then two distinct types of fluctuations are expected: Field of random sound waves that are irrotational (sound mode) and field of incompressible but rotational turbulence (vorticity mode) (Kovaszny 1950). For true sound waves, if the turbulence intensity is low, then the contribution of velocity perturbations to Mach number is insignificant. Hence, across the sound wave, the compressibility effects (pressure fluctuations) are of second order, in comparison with velocity (Kovaszny 1950). Under these assumptions, the rms density and velocity fluctuations can be estimated analytically from the known rms mass flux:

$$\frac{\overline{u'^2}}{\overline{u}^2} = \frac{(\overline{\rho u})'^2}{\overline{\rho u}^2} \left[ 1 - 2R_{Tu}(\gamma - 1)M^2 + (\gamma - 1)^2M^4 \right]^{-1} \quad (12a)$$

$$\frac{\overline{\rho'^2}}{\overline{\rho}^2} = (\gamma - 1)^2M^4 \frac{\overline{u'^2}}{\overline{u}^2} \quad (12b)$$

where  $R_{Tu}$  is shown to be almost constant and equal to  $-0.8$  in many transonic environments (Motallebi 1994). A more complete description of  $R_{Tu}$  dependence on flow conditions can be found in Stainback and Johnson (1983). Furthermore, analogous analytic expressions that include total temperature fluctuations are described in Motallebi (1994).

Finally, to generalize the discussed methodologies in a planar flow field, a probe with one or more inclined wires must be used. In contrast to normal wires, inclined wires have considerable angular sensitivity, and thus, Eq. 6 can be modified to include this effect (Motallebi 1994):

$$\frac{E'_b}{E_b} = S_\rho \frac{\rho'}{\rho} + S_u \frac{u'}{u} + S_{T_0} \frac{T_0'}{T_0} + S_\alpha \alpha' \quad (13)$$

where  $S_\alpha$  is the angular sensitivity defined as  $\partial \log E_b / \partial \alpha$  or alternatively:

$$S_\alpha = \frac{1}{2} \left( \frac{1}{\tau_{wr}} \frac{\partial \log \eta}{\partial \alpha} - \frac{\partial \log Nu}{\partial \alpha} \right). \quad (14)$$

In general, the added complexity due to the introduced angular dependency has encumbered accurate multidimensional measurements using conventional sensitivity analysis techniques, and results are reported to be inferior to that of a normal wire (Motallebi 1994).

## 2 Proposed methodology

The ultimate objective of the current research effort is to extend the basic low-speed cross-hot-wire calibration procedures (voltage-velocity-angle correlations) into the compressible subsonic and transonic flow regimes. This is mainly established through adaptations of normalized nondimensional parameters, which characterize the dependency of Nusselt number on Reynolds and Mach numbers. Universal empirical correlations for infinitely long wires are often used to predict qualitative trends; the present work, however, outlines a method to treat quantitative data by reducing its dependencies. Consequentially, so long as the mean (or if possible instantaneous) total temperature and local mean Mach number are supplied along with the wire voltages, the instantaneous mass flux and flow angle can be obtained via probe-specific calibrations consisting of a single compressibility corrected Nusselt–Reynolds relationship and a directional calibration curve. Although the technique is only verified within the compressible subsonic range ( $0.3 < M < 0.9$ ), the methodology may also hold true within the transonic regime ( $0.9 < M < 1.2$ ) as the functional dependencies are similar.

Among the main contributions of the article, this procedure enables the time accurate calculation of mass flux and flow angle “directly from calibration”. This is evident considering the instantaneous wire voltages are evaluated point-by-point on the calibration curves, absent of sensitivity-based analysis (Eq. 6). Moreover, if desired, under certain assumptions/conditions, the percent rms fluctuations of density and velocity may be estimated using Eqs. 12a, 12b from the already computed mass flux. In addition, as an addendum to the proposed methodology, sensitivities at local flow conditions can be calculated (Eqs. 8a, 8b, 8c) without additional calibration data; and the classical “sensitivity-based” fluctuation measurements can be performed to obtain instantaneous velocity and density independently.

### 2.1 Instrumentation

The cross-hot-wire is a probe designed in-house with short prongs, 2.5 and 1 mm in length, which also prevents prong vibrations during high-speed operation (Brunn 1995). The angle between the two wires is  $110^\circ$ , with a lateral distance on the order of 0.5 mm. The wires are 5 and  $9\ \mu\text{m}$  in diameter and made of platinum-coated tungsten, which have an optimum frequency response up to  $\sim 20$  and  $\sim 70$  kHz, respectively, spanning across a total length of about 2.5 mm, with an active length on the order of 1 mm, Fig. 1. The corresponding  $l_w/d_w$  ratios are acceptable with regard to conduction end loss, frequency response, spatial resolution and strength (Li 2001). Before calibration, the wires are pre-stressed and pre-heated at the

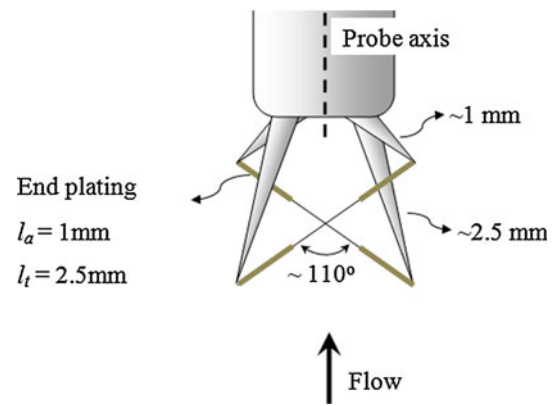
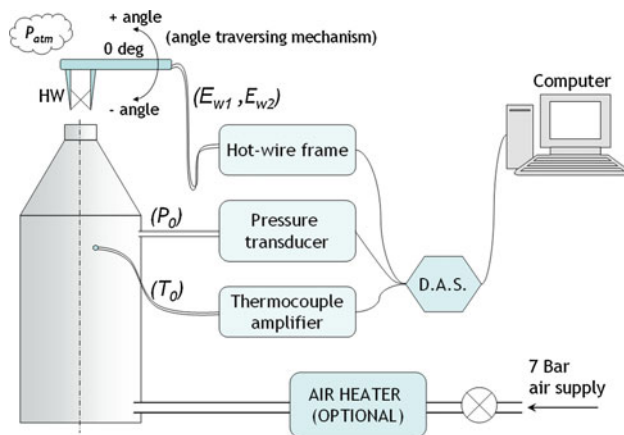


Fig. 1 Schematic of the cross-hot-wire probe

highest expected dynamic pressure and nominal wire temperature, to ensure that no additional strain is imposed that could alter the wire resistances during operation. In the course of this process, the wires are also checked for vibrations, which could generate detrimental strain gauging effects (Stainback and Nagabushana 1993). The anemometer system is a Dantec Streamline 90N10 Frame, which includes a controller circuit and supports up to six 90C10 CTA modules. Each CTA module has its own programmable signal conditioner capable of amplification, offsetting and analog low pass filtering, in this case imposed at 30 kHz. The system is initiated and operated by Dantec StreamWare® software. The frequency response is optimized by a square wave test at the highest observed velocity by adjusting the servo loop amplifier gain, filter cutoff and settings of the coils.

From the dimensional analysis for the heat transfer problem over a heated constant temperature wire under convection, the nondimensional parameters simplify to Reynolds number, Nusselt number and the Mach number, as presented in Eq. 4. If the flow field static and total pressures, in addition to the total temperature, are known, then it is possible to correlate the voltage across the wire with the fluid properties; even a simple open jet facility can satisfy these requirements. An open jet with contraction ratio of 25, exiting to atmospheric conditions, served as the calibration facility for the cross-hot-wire probe attached to a yawing mechanism. Flow of air is ensured through common 7 bar shop air supplied optionally through an electric air heater upstream. During calibration and verification procedures, exit total and static pressures are measured via pressure taps located prior to the area reduction and connected to a Validyne DP10 differential pressure transducer and a reference pressure transducer, Druck DPI 150 open to atmosphere. The total temperature is measured by two K-type thermocouples located within the nozzle. The acquired data is discretized by a 16bit NI-6251 data acquisition card with a maximum sampling frequency of



**Fig. 2** Schematic of the calibration facility

1.25 MHz. The facility and the measurement chain are sketched in Fig. 2.

## 2.2 Computation of nondimensional parameters

The Nusselt number is calculated from Eq. 1, where the convective heat transfer rate ( $q$ ) is obtained from the consumed power associated with wire Joule heating. For  $Re > 20$ , the conduction end losses diminish to relatively negligible amounts (Li 2001), in addition to being insignificant for wire-specific calibration procedures and thus:

$$q = \frac{E_w^2}{R_w}. \quad (15)$$

As the output voltage of a hot-wire anemometer is the bridge voltage ( $E_b$ ), the related wire voltage ( $E_w$ ) can be computed through the known resistance within the circuitry and the Nusselt number in terms of the bridge voltage can be written as (Nagabushana and Stainback 1992):

$$Nu = \frac{E_b^2}{k(T_w - \eta T_0)} \left( \frac{R_w}{\pi l_a (R_t + R_l + R_w)^2} \right) \quad (16)$$

where all resistances are constant for CTA operation. The precise values of those resistances are not strictly required since they only cause a fixed bias shift in the calculated Nusselt Number. In Eq. 16, the recovery factor ( $\eta$ ) term is obtained from empirical correlations (Dewey 1965) and thermal conductivity is computed using the 0.7 power law (George et al. 1989).

Mach number and static temperature (therefore velocity) are calculated from the isentropic flow relations when total pressure and temperature and the static pressure are known, whereas Reynolds number is calculated from Eq. 3 with density obtained from the ideal gas relation of free stream static quantities and the dynamic viscosity calculated using Sutherland's relation.

The selection of an appropriate evaluation temperature in computation of thermal conductivity and viscosity may have a significant effect on the respective calibration curve. In low-speed flows, the average conditions can be well represented by the film temperature defined as the average of the wire and total temperatures (George et al. 1989). However, in high subsonic and transonic speeds, the boundary layer around the wire becomes thinner and the total temperature itself may better represent the average conditions (Dewey 1965); hence, this definition is also implemented in the present study.

## 2.3 Determination of the wire temperature

During the computation of Nusselt number, using Eq. 16, the only remaining unknown is the mean wire temperature, which is merely a constant value in CTA mode. One of the possible ways to determine the wire temperature is using the resistance–temperature law:

$$\frac{R}{R_{ref}} = 1 + a_0(T_w - T_{ref}) + a_1(T_w - T_{ref})^2. \quad (17)$$

Although commonly employed via an oven, accurate knowledge of the coefficients  $a_0$  and  $a_1$  does not typically exist and the wire temperature computed from this relation may not necessarily be consistent with the imposed Nusselt number defining conditions.

A more precise way of determining the wire temperature is through widespread variation of a least square fitted free parameter (George et al. 1989; Yasa et al. 2005). Considering the negligible Mach number dependency of Nusselt number at low speeds in Eq. 4, for a given flow angle, the correct wire temperature must collapse a population of  $Re$ - $Nu$  data into a single curve. By calculating the Nusselt number for a range of presumed wire temperatures, the best data cloud collapsing value determines the *effective* wire temperature. Specifically, the level of data scatter is quantified by the  $R^2$  value of a fitted 4th order polynomial, recommended by George, et al. (1989), Fig. 3.

To prevent large errors, a priori determined wire temperature, and thus resistance, must be kept constant throughout the calibration and proceeding measurements. This can only be satisfied by keeping the hot resistance, not overheat ratio, constant. Furthermore, to prevent detrimental effects of aging due to oxidation of the wire material, where the wire resistance temperature relationship is amended, the mean wire temperature should be kept below 525 K for platinum-coated tungsten wires (Brunn 1995). It has been observed that through consecutive initializations with varying initial ambient temperatures, up to 330 K, and at different operational life spans of the wire, the computed wire temperature remained the same within

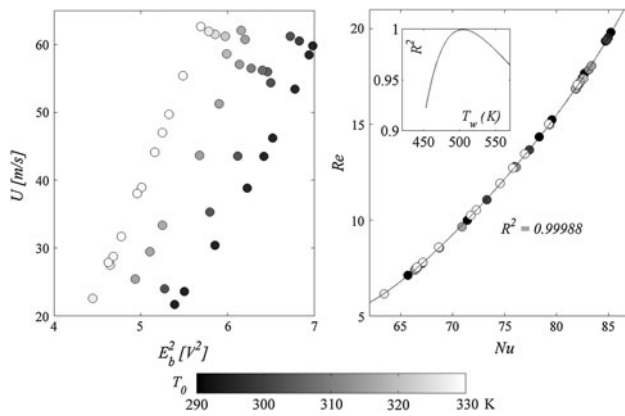


**Fig. 3** Determination of wire temperature by flow condition variation via  $Re$ – $Nu$  relationship

2 K. Therefore, although commonly desirable, the need for in situ calibration is eliminated.

### 2.4 Mass-flux calibration

Once the wire temperature is known, the mass-flux calibration at reference angular position (the probe axis, Fig. 1) can be performed in the operational velocity range (high subsonic) by recording total pressure and temperature, static pressure and wire voltages, and thus calculating local  $Nu$ ,  $Re$  and  $M$ . In an effort to eliminate the Mach number dependency of the measured Nusselt number, Dewey’s empirical correlation for flow normal infinitely long wires (Dewey 1965) can be partly adapted to compensate for the compressibility effects. By rearranging the terms in Dewey (1965):

$$Nu(Re, \infty) = \frac{Nu(Re, M)}{\varphi(Re, M)} \tag{18}$$

where  $Nu(Re, M)$  is the Nusselt number,  $Nu(Re, \infty)$  is the Mach independent Nusselt number obtained from supersonic flow correlations and  $\varphi(Re, M)$  is the term which quantifies deviation from supersonic relations.  $\varphi$  is given by:

$$\varphi(Re, M) = 1 + A(M) \left[ 1.834 - 1.634 \left( \frac{Re^{1.109}}{2.765 + Re^{1.109}} \right) \right]$$

$$x \left[ 1 + \left( 0.3 - \frac{0.0650}{M^{1.670}} \right) \left( \frac{Re}{4 + Re} \right) \right] \tag{19a}$$

$$A(M) = \frac{0.6039}{M} + 0.5701 \left[ \left( \frac{M^{1.222}}{1 + M^{1.222}} \right)^{1.569} - 1 \right]. \tag{19b}$$

By using this correction term  $\varphi$ , the Mach effect on Nusselt number can be diminished, Eq. 18, and thus any real wire heat–momentum transfer relationship can be

decoupled from compressibility effects if the local mean Mach number is known. Since 5 % deviation of Mach number merely corresponds to 1 % error in the resultant mass flux, derived from a typical calibration curve (Fig. 4), the Mach number fluctuations can be considered insignificant in most measurement environments.

On the other hand, Dewey proposed the empirical correlations for flow normal wires; hence, applicability to slanted wires is ambiguous due to the angular effect. Within the scope of this investigation, since the Mach number is utilized to purely compensate for compressibility effects and the major flow information is propagated by the Reynolds effect, it is concluded that the optimum choice is to use wire normal Reynolds number and flow Mach number in  $\varphi$  factor computation.

As a result, the calibration is conducted for  $Re$  versus  $Nu_{corr}$ , which is a Mach independent single curve, the validity of which was investigated for 5 and 9  $\mu\text{m}$  wires, at several fixed overheat ratios and a wide range of free stream total temperatures and velocities. A typical temperature and velocity variant data set is presented in Fig. 4 (left), where the charted  $Re$ – $Nu$  relationship yields to a scatter of the data, as large as 10 % from the local mean. In contrast, with the Mach corrected Nusselt relation, Fig. 4 (right), the scatter in the data is eliminated. Consequently, the correction term  $\varphi$  is examined for a broad range  $20 < Re_{dw} < 200$ ,  $0.3 < M < 0.9$ , and a flow total temperature variation driven overheat shift of  $\Delta\theta = 0.3$  at  $\theta > 1.3$ . It is demonstrated that the term eliminates the Mach number dependency, independent of overheating, within  $\pm 0.4\%$ . The resultant calibration curve successfully represents the wire heat transfer characteristics, demonstrating the independence from flow conditions; hence, only a cold calibration is sufficient to establish the wire-specific heat–momentum transfer relation.

During measurements, since this  $\varphi$  factor includes the Reynolds and Mach numbers, despite the Reynolds number being the dependent variable in the calibration curve, an iterative procedure is deemed necessary.

### 2.5 Angular calibration

The angular response of the cross-hot-wires is investigated in the same flow range,  $20 < Re_{dw} < 200$ ,  $0.3 < M < 0.9$ ,  $\Delta\theta = 0.3$  for  $\theta > 1.3$ , with yaw variation of  $-30 < \alpha < 30$ . To deduce the flow angle information from the two recorded wire voltages, the *effective* Reynolds number, the one that yields to the same Nusselt number if the probe was aligned at the reference position, is calculated for each of the wires using their respective mass-flux calibration curves (Figs. 4, 5).

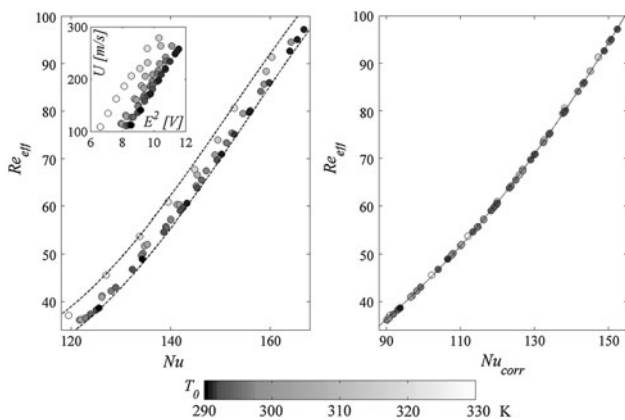


Fig. 4 Establishing mach number independent  $Re-Nu$  relationship

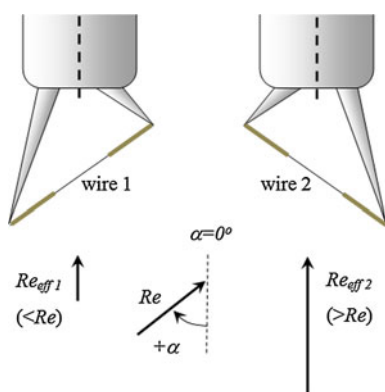


Fig. 5 Effective Reynolds number on each wire at fixed flow angle

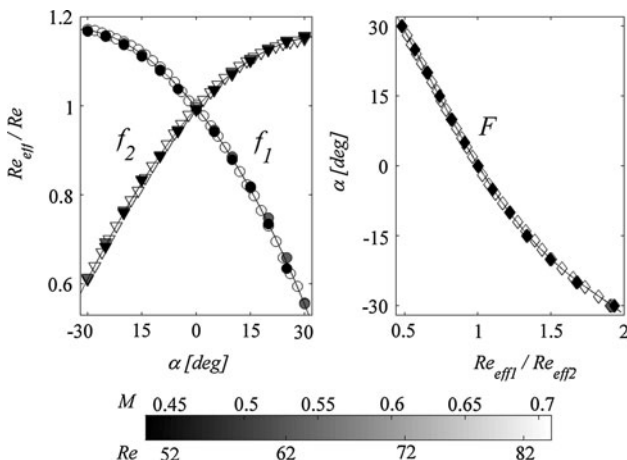


Fig. 6 Angular dependency of hot-wire at various  $Re$  and  $Ma$

The relation between the actual and effective Reynolds numbers can be represented by a function, which is obtained during the angular calibration, Fig. 6:

$$Re_{eff} = Re \cdot f(\alpha). \tag{20}$$

In the most general sense,  $f(\alpha)$  could be a function of Reynolds and Mach numbers. However, as presented in Fig. 6, in the scope of the present investigation, no systematic angular response variation is observed based on Reynolds or Mach dependency, indicated by the single angular calibration curve characterizing the behavior at all flow conditions, in agreement with Motallebi (1994) and Smits and Muck (1984). Furthermore, lack of a spread in data for various flow temperatures supports the negligible overheating ( $\theta$ ) dependence assumption for moderate changes in  $T_0$ ,  $\sim 40$  K. Thus, a curve fit, in this case a 4th order polynomial, can represent the angular response for all Mach and Reynolds numbers. As a result, during measurements, the two unknowns, Reynolds number and flow angle, can be acquired by the  $2 \times 2$  system of equations constituted of Eq. 20 for each wire, yielding to:

$$\alpha = F\left(\frac{Re_{eff1}}{Re_{eff2}}\right). \tag{21}$$

By this formulation, the ratio of the effective Reynolds numbers of the two wires directly provides the flow angle, Fig. 6.

It may be worthwhile to note that yawing the probe causes the flow to become more perpendicular to one of the wires; hence, the effective Reynolds number becomes larger than the actual Reynolds number for that wire. At the high extremity of the mass-flux calibration curve, Fig. 4, the greater than actual/real effective Reynolds number can go beyond the limits of the mass-flux calibration curve. Although impractical in high-speed flows, the usual practice in low-speed applications is by constructing the calibration curve up to a velocity, which is sufficiently higher than the maximum expected value. In the present methodology, considering the Mach and Reynolds independence of the angular calibration curve, superficial non-error producing  $Re_{eff}-Nu$  points are generated outside the range of the original mass-flux calibration at both extremities to satisfy these requirements.

Concisely, the primary benefit of the effective Reynolds approach is the elimination of full multidimensional mappings of combined Mach, Reynolds and angular response. The validity of the angular calibration in Fig. 6 is verified by recovering the calibration data from the fitted solution, which displayed a low level of scatter, the 95 % confidence level within  $\pm 0.4^\circ$  and  $\pm 0.6$  % for  $\alpha$  and  $Re$  respectively.

### 2.6 Methodology overview

A brief breakdown of the calibration and experimental data processing methodology can be found in Fig. 7. Having determined the wire temperatures initially, by varying the velocity of a cold jet and recording the HW bridge voltages at reference probe position along with flow total pressure

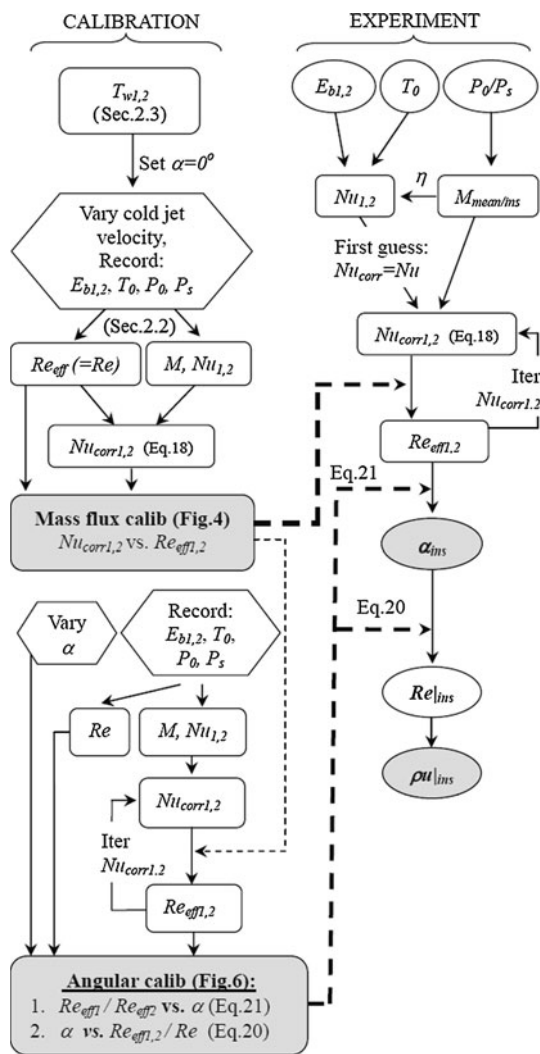


Fig. 7 Calibration and data processing methodology overview

and temperature in addition to static pressure, the mass-flux calibration can be achieved. To be able to characterize the angular dependency, the same cold jet facility is operated for different hot-wire yaw angles, recording the flow quantities at arbitrary conditions due to the Mach and Reynolds independency of the curves. The obtained calibration maps, characterizing both the mass flux and the angular response of the cross-hot-wire, are universal for the given probe in a sense that validity is independent of surrounding flow total temperature and pressure, static pressure, and consequently local Mach number.

Placing the probe in a measurement environment where entropy (total temperature) fluctuations are not significant, and recording the two hot-wire voltages, in addition to the mean local Mach number and total temperature, using the mass-flux and angular calibrations, the instantaneous planar flow angle and mass flux may be obtained. If desired, as a corollary of the proposed methodology, the instantaneous

density and velocity can be computed in cohesion with the sensitivity analysis, as thoroughly discussed in Chapter 3. Alternatively, for flow conditions where the sound mode is dominant (irrotational flow field), and if the turbulence intensity is low, the instantaneous mass flux and flow angle can be analytically decomposed into rms density and velocity fluctuations via Eqs. 12a, 12b.

In conclusion, the provided methodology presents an accurate, generalized, straightforward pathway for calibrating and processing cross-hot-wire signals under compressible subsonic and transonic conditions, in the absence of added complexities/uncertainties associated with closed loop wind tunnels and direct methods. Although primarily geared toward flows with negligible total temperature fluctuations, the suggested technique can be extended by utilizing a CCA at low overheat, in conjunction with the CTA's, to compensate for high frequency changes in total temperature via substitution into Eq. 16.

### 2.6.1 Verification

In an attempt to validate the calibration/processing methodology, a posteriori cross-hot-wire measurements are conducted in the same calibration jet facility with known static quantities, Fig. 2. The imposed mean mass flux and angle are compared with the values computed from the post-processing procedures, using the calibration curves as outlined in Fig. 7. Table 1 depicts the low deviation between the imposed and hot-wire calculated quantities and reflects the robustness of the methodology for all operating conditions independent of  $T_0$ ,  $\theta$ ,  $\rho u$ ,  $\alpha$ . The maximum observed discrepancy among the two different sources is found to be 0.67 %, 0.5° in mean mass flux and yaw angle, respectively.

### 2.7 Uncertainty analysis

Hot-wire measurements are subjected to both random and systematic sources of errors, such as uncertainties associated with HW voltage, total/static pressure ratio, total temperature and calibration curve-fitting errors. The cumulative error can

Table 1 Validation of measurement technique

| $T_0$ | $\theta$ | $\rho u$ (kg/m <sup>2</sup> s) |       |       | $\alpha$ (°) |        |
|-------|----------|--------------------------------|-------|-------|--------------|--------|
|       |          | Jet                            | HW    | % Dif | Jet          | HW     |
| 292 K | 1.67     | 344.2                          | 341.9 | 0.67  | 0            | -0.05  |
| 290 K | 1.68     | 276.9                          | 276.7 | 0.09  | 0            | -0.17  |
| 292 K | 1.67     | 229.1                          | 229.5 | -0.19 | 0            | 0.09   |
| 315 K | 1.55     | 280.5                          | 278.9 | 0.55  | -20          | -19.53 |
| 289 K | 1.69     | 313.3                          | 313.1 | 0.06  | 20           | 20.43  |

be estimated as the root mean square of the standard deviation quantities:

$$\Delta Re = \left[ \left( \frac{\partial f_1(\alpha)}{\partial \alpha} \Delta \alpha \right)^2 + \varepsilon_{\text{cfit1}}^2 \right]^{0.5} \quad (22a)$$

$$\Delta \alpha = \left[ \left( \frac{\partial f_2(Re_{\text{eff1}}/Re_{\text{eff2}})}{\partial (Re_{\text{eff1}}/Re_{\text{eff2}})} \Delta (Re_{\text{eff1}}/Re_{\text{eff2}}) \right)^2 + \varepsilon_{\text{cfit2}}^2 \right]^{0.5} \quad (22b)$$

$$\Delta Re_{\text{eff}} = \left[ \left( \frac{\partial f(Nu, M)}{\partial Nu} \Delta Nu \right)^2 + \left( \frac{\partial f(Nu, M)}{\partial M} \Delta M \right)^2 + \varepsilon_{\text{cfit3}}^2 \right]^{0.5} \quad (22c)$$

where  $\varepsilon_{\text{cfit}}$ 's are calibration curve-fitting errors and  $\Delta Nu$ ,  $\Delta M$ ,  $\Delta (Re_{\text{eff1}}/Re_{\text{eff2}})$  are computed from uncertainties of the directly measured quantities,  $\Delta E_b$ ,  $\Delta T_0$ ,  $\Delta (P_0/P_s)$ . Similarly, the derivatives are obtained by numerically perturbing the physically measured parameters due to the complexity associated with the direct mathematical formulations. The uncertainties are presented in the 95 % confidence level.

This analysis illustrates that the largest uncertainty contributor is the total temperature measurements where a  $\pm 1$  K uncertainty causes an uncertainty of  $\pm 1.1^\circ$  in yaw angle and  $\pm 2$  % in mass flux. The curve-fitting errors result in an uncertainty of  $\pm 0.8^\circ$  in flow angle and  $\pm 1.2$  % in mass flux. The smallest contribution is generated by uncertainties associated with voltage readings and total/static pressure measurements (therefore the Mach number) where  $\pm 0.25$  kPa error in pressure and even  $\pm 2$  mV error in voltage (estimated max white noise) cause an uncertainty of  $\pm 0.3^\circ$  in yaw angle and  $\pm 0.6$  % in mass flux.

Therefore, combinations of these uncertainties cause a total *absolute* accuracy error of  $\pm 1.4^\circ$  in yaw angle and  $\pm 2.5$  % in mass flux within the 95 % confidence level. These uncertainties can significantly be reduced if total temperature is measured more accurately, for example, the reduction of total temperature error down to  $\pm 0.5$  K results in cumulative yaw angle and mass-flux uncertainties of  $\pm 1.2^\circ$  and  $\pm 1.7$  %, respectively. For flow normal wire measurements, mass-flux uncertainty is  $\pm 2$  % for  $\pm 1$  K error and  $\pm 1.3$  % for  $\pm 0.5$  K error.

Uncertainty in turbulent fluctuation quantities, such as mass-flux intensity, can be estimated by assuming that errors diminish for pure fluctuations and the uncertainty is mostly propagated from the drift in the mean value. Therefore, for all nominal mass fluxes, fluctuation intensity uncertainty is in the order of  $\pm 2.56$  % for  $\pm 1$  K total temperature error. Uncertainty in angle fluctuation is negligible since it is not a strong function of the mean quantities, considering the locally linear behavior of the angular response within a mean value change of  $\pm 1.4^\circ$ .

### 3 Extension to sensitivity analysis

#### 3.1 Calculation of instantaneous density and velocity

Upon this point, the sensitivity-based data reduction techniques have not been utilized; instead, a mass flux and flow angle calculation method based on direct point-by-point evaluation of wire voltages on the nondimensional calibration curves was proposed. If the independent temporal variation in velocity and density is of interest, the conventional sensitivity analysis can be optionally extended to be used in conjunction with the present calibration scheme. Using the two inclined wires in a flow where  $T_0$  variations result in low percent fluctuations, rearranging Eq. 13 yields to:

$$\frac{E'_b}{E_b} - S_\alpha \alpha' = S_\rho \frac{\rho'}{\rho} + S_u \frac{u'}{u} \quad (23)$$

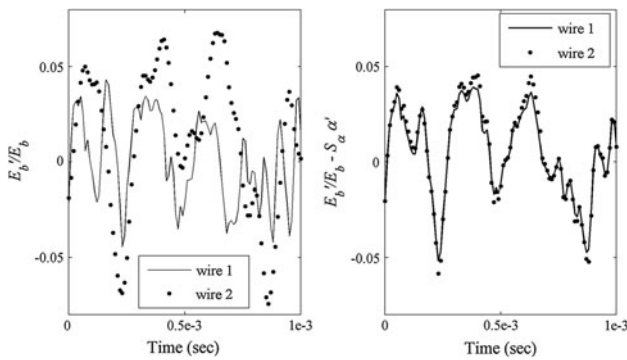
with  $S_\alpha$ ,  $S_u$ ,  $S_\rho$  sensitivities computed at a given data point by Eqs. 8a, 8b, 8c and 14 using mass-flux and angular calibrations of Figs. 4 and 6. Furthermore, for two wires with different  $S_{T_0}$ , a function of both wire overheat and diameter, if the independent computation of instantaneous mass flux from the each wire, Eq. 20, results in the same temporal distribution, then assumption of neglecting  $T_0$  fluctuations is validated (Smits et al. 1983; Motallebi 1994). Considering the prior known instantaneous angle variations, the only remaining unknowns are independent velocity and density perturbation quantities, hence the solution matrix of this  $2 \times 2$  system.

Figure 8 presents the two raw bridge voltages, in the presence and absence of the angular term. It is clear that the voltages are only correlated with the angular compensation. In the case of cross-hot-wires, since the angular sensitivity affects the two wires in opposite senses (close to and further away from wire normal flow direction), this compensation is demonstrated to be imperative.

#### 3.2 Wire sensitivity analysis

One of the challenges in utilizing sensitivity methods is acquiring a nonsingular solution matrix, a function of the wire-to-wire  $S_\rho/S_u$  variation. At several overheat ratios ( $\theta$  ranging from 1.42 to 1.70), the mass-flux-calibration-based sensitivities are calculated for  $9\mu$  wires under different flow conditions, Table 2. Despite large changes in overheating parameter, the resulting change in density–velocity sensitivity ratio is limited to 8 %; therefore, it is difficult to make the solution matrix (Eq. 23) well conditioned by solely varying overheat ratio.

On the other hand, considering  $Kn$  dependency of heat transfer, another possibility is utilizing two wires of different diameter (Jones et al. 1989) to ensure larger



**Fig. 8** Angular compensation in sensitivity analysis

**Table 2** Wire sensitivities at various flow conditions

|                      | $\theta$ | $S_\rho$ | $S_u$ | $S_{T_o}$ | $S_\rho/S_u$ |
|----------------------|----------|----------|-------|-----------|--------------|
| $M = 0.70, Re = 140$ | 1.42     | 0.280    | 0.234 | -1.10     | 1.197        |
|                      | 1.53     | 0.268    | 0.210 | -0.77     | 1.276        |
|                      | 1.70     | 0.277    | 0.215 | -0.60     | 1.288        |
| $M = 0.55, Re = 110$ | 1.42     | 0.285    | 0.210 | -1.15     | 1.357        |
|                      | 1.53     | 0.276    | 0.194 | -0.84     | 1.423        |
|                      | 1.70     | 0.280    | 0.200 | -0.58     | 1.400        |

variations within the system matrix. Figure 9 depicts the  $S_\rho, S_u$  variation at a range flow conditions, with a cross-hot-wire formed of 5 and 9  $\mu\text{m}$  diameter wires, indicating a wire-to-wire change in  $S_\rho/S_u$  up to 20 %. This effect of divergence from matrix singularity is further amplified in the vicinity of  $M = 0.6$ , reasonable considering that the heat transfer is Mach independent at very low subsonic and above transonic conditions, forcing a constant  $S_\rho/S_u$  ratio of 1. Additionally, Fig. 9 results are found to be in agreement with Nagabushana and Stainback (1992).

### 3.3 Experimental verification of the separation procedure

In an attempt to decouple instantaneous velocity and density fluctuations in free stream flow conditions, tests are conducted within the core of a free jet, as well as downstream of a 20 blade rotating flow perturbator (typical in turbomachinery applications), both at  $M = 0.7$  and  $Re_{9\mu\text{m}} = 125$ . For the latter case, the typical bridge voltage power spectra encountered during measurements can be found in Fig. 10, indicating the high frequency response of the probe, limited by the analog filter at 30 kHz, with distinct peaks at once per revolution, blade passing and its harmonics.

Figure 11a depicts the directly computed distribution of  $(\rho u)'$  and  $\alpha'$  along with sensitivity calculated  $\rho', u', \rho'u'$  for the measurements conducted at the exit of a jet core. The mass-flux intensity and  $\alpha'_{\text{rms}}$  are 0.63 % and  $0.56^\circ$ ,

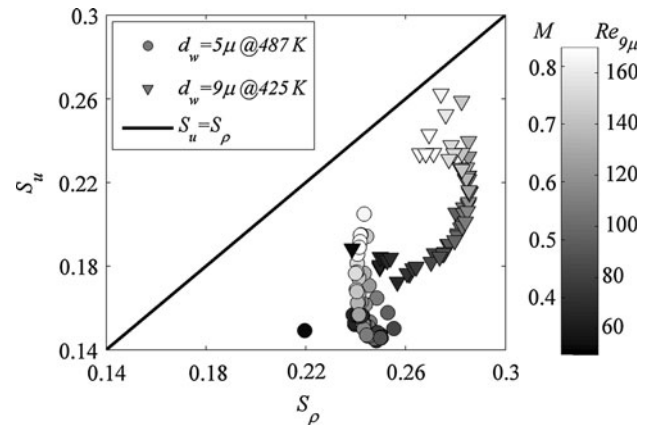


**Fig. 9** Sensitivity to velocity and density at various flow conditions

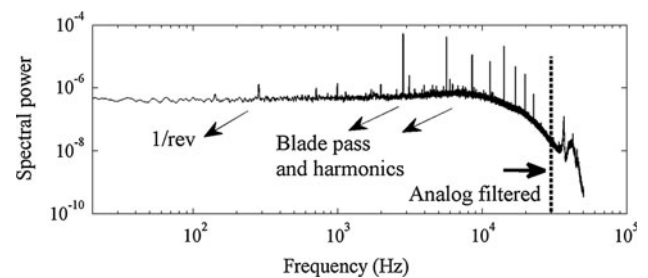


**Fig. 10** Typical bridge voltage power spectra

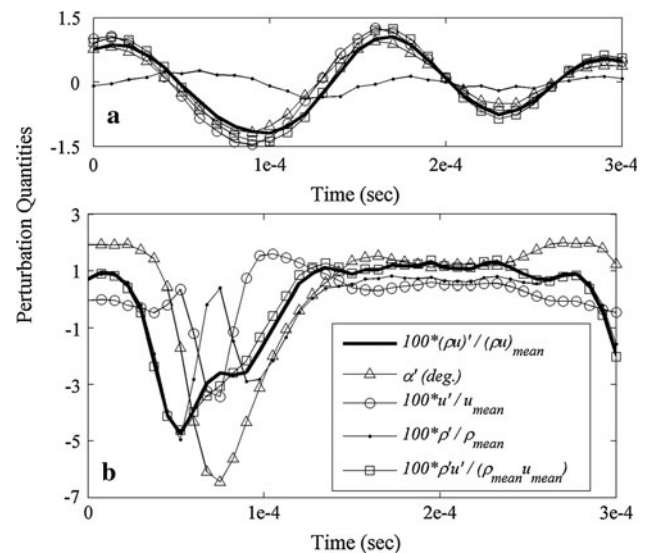


**Fig. 11** Typical perturbation—Core of a free Jet (a), downstream of a flow perturbator (b)

respectively, and there exists a high degree of correlation among instantaneous mass-flux, velocity and angle fluctuations. Moreover, the instantaneous mass-flux fluctuations calculated from the two different methods, directly from calibration  $(\rho u)'$  and sensitivity-based  $\rho'u'$ , display a high

degree of quantitative correlation. In addition, comparing the analytic decomposition of velocity and density rms quantities, Eqs. 12a, 12b, with the sensitivity decoupled values, Eq. 23, the results reveal large similarity,  $u_{\text{nrms}} = 0.61\%$ ,  $0.72\%$ ,  $\rho_{\text{nrms}} = 0.14\%$ ,  $0.13\%$ , respectively, in part validating both the proposed technique and instantaneous density–velocity decoupling. This is encouraging considering the sound mode (the principal assumption of Eqs. 12a, 12b) is expected to be the dominant turbulence feature in this type of flow environment.

In the case of measurements conducted downstream of the rotating perturbator application, Fig. 11b, it is clear that the two instantaneous mass-flux fluctuations, calculated based on direct and sensitivity analysis methods, still prove to provide similar behaviors. Interestingly, the density fluctuations,  $\rho'$ , seem to correlate moderately well with mass-flux variations. This could be due to the perturbator generated variations in static pressure sweeping the location of the probe in the circumferential direction, yielding a flow more prone to streamwise compression. On the other hand, velocity perturbations,  $u'$ , indicate a similarity in trend with flow angle,  $\alpha'$ , typical behind rotating perturbators, conceivably an indication of perturbator driven rotational vorticity field. Quantifying the data in terms of averaged perturbation quantities, the computed mass-flux intensity and  $\alpha_{\text{rms}}$  are  $1.52\%$  and  $2.53^\circ$ . The analytic and sensitivity analysis based computations of rms velocity and density provide  $u_{\text{nrms}} = 1.35, 1.31\%$  and  $\rho_{\text{nrms}} = 0.25, 1.36\%$  respectively. Although the  $u_{\text{nrms}}$  quantities relate reasonably well, the rms density perturbations seem highly inconsistent. This may be an artifact of the dominant vorticity mode present downstream of the flow perturbator; the analytical solution of  $u_{\text{nrms}}$  and  $\rho_{\text{nrms}}$ , Eqs. 12a, 12b, is valid for true sound waves, in the absence of rotational turbulent structures (Kovasznay 1950), possibly violated in this circumstance.

#### 4 Conclusions

A novel, practical, and accurate procedure is developed for conducting high-speed cross-hot-wire calibration and data reduction, combining wire-specific data with trends observed for infinitely long wires. Through nondimensionalization of the physical parameters in the form of Nusselt, Reynolds and Mach numbers, and via compressibility normalization by which the Mach independency is established, the mass-flux calibration yields to a well-collapsed single curve. It has been demonstrated that calibrations obtained in a cold jet (e.g.,  $T_0 = 290$  K) are valid at measurement environments where the temperature is elevated (e.g.,  $T_0 = 335$  K). Angular response of the probe is investigated by means of effective Reynolds number concept, and it has shown that a single

angular calibration curve represents the behavior at all flow conditions. The calibration and measurements are validated for  $20 < Re_{\text{dw}} < 200$ ,  $0.3 < M < 0.9$ ,  $-30^\circ < \alpha < 30^\circ$  and  $\Delta\theta = 0.3$  at  $\theta > 1.3$ . Moreover, due to the similarity of functional relationships, the technique is expected to maintain its validity within the transonic regime ( $0.9 < M < 1.2$ ).

Alternatively, the calibration methodology can also be used to obtain the wire sensitivities in a reliable, practical manner. Using the instantaneous angle information obtained from the proposed methodology, instantaneous density and velocity fluctuations may be independently computed.

In conclusion, the new data reduction methodology offers a high-speed calibration scheme over a wide range of Reynolds and Mach numbers with an effort equivalent to that of a cross-hot-wire calibration under isothermal low-speed flows. As nondimensional parameters and widely accepted correlations are used, there is no need for closed loop wind tunnels, which vary each flow variable independently. Moreover, as the procedure is based on general heat transfer law, applicability could be extended to CCA and CVA provided that the wire temperature resistance law is well quantified.

#### References

- Behrens W (1971) Total temperature thermocouple probe based on recovery temperature of circular cylinder. *Int J Heat Mass Transf* 14(10):1621–1630
- Brunn HH (1995) Hot-wire anemometry: principles and signal analysis. Oxford University Press, New York
- Dewey CF (1961) Hot-wire measurements in low Reynolds number hypersonic flows. *ARS J* 28(12):1709–1718
- Dewey CF (1965) A correlation of convective heat transfer and recovery temperature data for cylinders in compressible flow. *Int J Heat Mass Transf* 8(2):245–252
- George WK, Beuther PD, Shabbir A (1989) Polynomial calibrations for hot-wires in thermally varying flows. *Exp Thermal Fluid Sci* 2(2):230–235
- Horstman CC, Rose WC (1975) Hot-wire anemometry in transonic flow. NASA-TM-X-62495
- Johnson DA, Rose WC (1976) Turbulence measurements in a transonic boundary layer and free shear flow using laser velocimetry and hot-wire anemometry techniques. AIAA-76-0399
- Jones GS, Stainback PC, Harris CD, Brooks CW, Clukey CB (1989) Flow quality measurements for the langley 8-foot transonic pressure tunnel LFC experiment. AIAA-89-0150
- Kegerise MA, Spina EF (2000) A comparative study of constant-voltage and constant-temperature hot-wire anemometers. *Exp Fluids* 29(2):154–177
- Kovasznay LS (1950) Hot-wire anemometer in supersonic flow. *J Aeronaut Sci* 17(9):565–572, 584
- Kovasznay LS (1953) Turbulence in Supersonic Flow. *J Aeronaut Sci* 20(10):657–674, 682
- Li JD (2001) An investigation on the length to diameter ratio of hot wire filament in turbulence measurements. In: 14th Australasian fluid mechanics conference
- Lord RG (1974) Hot-wire probe end-loss corrections in low density flows. *J Phys E: Sci Instrum* 7(1):56–60

- Mikulla V, Horstman CC (1975) Turbulence stress measurements in a nonadiabatic hypersonic boundary layer. *AIAA J* 13(12):1607–1613
- Morkovin MV (1956) Fluctuations and hot-wire anemometry in compressible flows. *AGARDograph* 24
- Motallebi F (1994) A review of the hot-wire technique in 2-D compressible flows. *Progr Aeros Sci* 30(3):267–294
- Nagabushana KA, Stainback PC (1992) Heat transfer from cylinders in subsonic slip flows. *NASA-CR-4429*
- Rong BS, Tan DM, Smits AJ (1985) Calibration of the constant temperature normal hot-wire anemometer in transonic flow. *MAE-1696*, Princeton University
- Rose WC, McDaid EP (1977) Turbulence measurement in transonic flow. *AIAA J* 15(9):1368–1370
- Smits AJ, Muck KC (1984) Constant temperature hot-wire anemometer practice in supersonic flows, part 2: the inclined wire. *Exp Fluids* 2:33–41
- Smits AJ, Hayakawa K, Muck KC (1983) Constant temperature hot-wire anemometer practice in supersonic flows, part 1: the normal wire. *Exp Fluids* 1(2):83–92
- Spangenberg WG (1955) Heat-loss characteristics of hot-wire anemometers at various densities in transonic and supersonic flow. *NACA-TN-3381*
- Stainback PC, Johnson CB (1983) Preliminary measurements of velocity, density and total temperature fluctuations in compressible subsonic flow. *AIAA-83-0384*
- Stainback PC, Nagabushana KA (1993) Review of hot-wire anemometry and the range of their applicability. In: *Third International Symposium on Thermal Anemometry*, ASME Fluids Engineering Division Summer Meeting, vol 167, pp 93–134. Washington DC
- Stainback PC, Nagabushana KA (1995) Reinvestigation of hot-wire anemometry applicable to subsonic compressible flows using fluctuation diagrams. *J Fluids Eng* 117(2):263–269
- Walker DA, Ng WF, Walker MD (1988) Experimental comparison of two hot-wire techniques in supersonic flow. *AIAA J* 27(8):1074–1080
- Yasa T, Paniagua G, Denos R (2005) Hot-Wire anemometry for non-isothermal flows and effect of aging of the sensor wire. *Data acquisition and signal processing for turbomachinery applications*. Von Karman Institute for Fluid Dynamics